

Surrogate MR markers of response to chemo- or radiotherapy in association with co-treatments: a retrospective analysis of multi-modal studies

Bénédicte F. Jordan^a and Bernard Gallez^{a*}

The study of magnetic resonance (MR) markers over the past decade has provided evidence that the tumor microenvironment and hemodynamics play a major role in determining tumor response to therapy. The aim of the present work is to predict and monitor the efficacy of co-treatments to radio- and chemotherapy by noninvasive MR imaging. Ten different co-treatments were involved in this retrospective analysis of our previously published data, including NO-mediated co-treatments (insulin and isosorbide dinitrate), anti-inflammatory drugs (hydrocortisone, NS-398), anti-angiogenic agents (thalidomide, SU5416 and ZD6474), a vasoactive agent (xanthinol nicotinate), botulinum toxin and carbogen breathing. Dynamic contrast enhanced (DCE) MRI, intrinsic susceptibility-weighted (BOLD) MRI and electronic paramagnetic resonance (EPR) oximetry all reflect tumor microenvironment hemodynamic variables that are known to influence tumor response. Eight MR-derived parameters (markers) were tested for their ability to predict therapeutic outcome (factor of increase in regrowth delay) in experimental tumor models (TLT and FSall) after radiation therapy and/or chemotherapy with cyclophosphamide, namely tumor pO_2 and O_2 consumption rate (using EPR oximetry); tumor blood flow and permeability, i.e. V_p , K_{trans} , K_{ep} and percentage of perfused vessels (using DCE-MRI); and BOLD signal intensity and R_2^* (using functional MRI). This multi-modal comparison of co-treatment efficacy points out the limitations of each MR marker and identifies *in vivo* pO_2 as a relevant endpoint for radiation therapy. DCE parameters (V_p and K_{ep}) were identified as a relevant endpoints for cyclophosphamide chemotherapy in our tumor models. This study helps qualify relevant imaging endpoints in the preclinical setting of cancer therapy. Copyright © 2010 John Wiley & Sons, Ltd.

Keywords: surrogate marker; MRI; EPR; tumor; multi-modal; imaging endpoint; theranostics

1. INTRODUCTION

The study of magnetic resonance (MR) markers over the past decade has provided evidence that the tumor microenvironment and hemodynamics play a major role in determining tumor response to radiation therapy or chemotherapy (1,2). Indeed, tumor hypoxia is considered to be a therapeutic problem, as it makes solid tumors resistant to ionizing radiation and some forms of chemotherapy (3). This has recently been illustrated in a large clinical trial, where J. Overgaard (4) identified 10 108 patients in 86 randomized trials designed to modify tumor hypoxia in patients treated with curative attempted primary radiation therapy alone. Overall modification of tumor hypoxia significantly improved the effect of radiotherapy for the outcome of loco-regional control and with an associated significant overall survival benefit. Therefore, the predictive value of MR markers of response to treatment is of crucial importance in the management of cancer patients in order to improve the therapeutic index by allowing better individualization of treatment. In parallel, innovative therapies able to modulate the microenvironment such as flow and oxygenation are currently being developed in order to improve treatment outcome, which also need preclinical validation using surrogate MR markers (5–7).

Tumor hypoxia results from an imbalance between oxygen delivery and oxygen consumption, either of which may be

potentially targeted by therapeutic interventions. On the one hand, tumor oxygenation may be improved by an increase in oxygen supply, including approaches such as carbogen breathing, hyperthermia, administration of vasoactive drugs or modifiers of Hb affinity or of oxygen transport capacity (6). On the other hand, tumor oxygenation may be increased by reducing the rate of oxygen consumption by tumor cells, as predicted theoretically by Secomb *et al.* (8). His simulation showed that modification of oxygen consumption could be much more efficient at alleviating hypoxia than modification of oxygen delivery. Several pharmacological drugs that inhibit cellular oxygen consumption have been successfully characterized for their ability to increase tumor oxygenation *in vivo*, including meta-iodobenzylguanidine (9), insulin (10), anti-inflammatory drugs (11), corticoids (12), some antagonists of vascular

* Correspondence to: B. Gallez, CMFA/REMA, Avenue Mounier 73.40, B-1200 Brussels, Belgium.
E-mail: bernard.gallez@uclouvain.be

^a B. F. Jordan, B. Gallez
Laboratory of Biomedical Magnetic Resonance, Louvain Drug Research Institute, Université Catholique de Louvain, Avenue Mounier 73, B-1200 Brussels, Belgium

Table 1. List of co-treatments with their respective dose, vehicle and injection route, and imaging methods, tested in combination with either radio- or chemotherapy

Co-treatment	Dose	Vehicle or speciality	Injection route	Treatment	Imaging method					Ref.
					Oximetry	O ₂ consumption	DCE-MRI	BOLD (fMRI)	EPR	
Insulin	400 mU/kg	Actrapid HM	i.v.	Radiotherapy (n = 6)	n = 5	n = 4	n = 5	n = 6	n = 6	(10)
Isosorbide dinitrate	0.2 mg/kg	Saline	i.p.	Radiotherapy (n = 6)	n = 5	n = 4	/	n = 9	n = 9	(16)
Hydrocortisone	7.7 mg/kg	Saline	i.p.	Radiotherapy (n = 5)	n = 5	n = 5	n = 6	—	—	(12)
NS-398	10 mg/kg	DMSO	i.p.	Radiotherapy (n = 6)	n = 7	n = 4	n = 5	n = 5	n = 5	(11)
Thalidomide	200 mg/kg daily	DMSO	i.p.	Radio/chemo (n = 5/5)	n = 8	—	n = 5	—	—	(54)
SU-5416	25 mg/kg daily	DMSO	i.p.	Radio/chemo (n = 6/5)	n = 4	n = 6	n = 7	—	—	(13)
ZD-6474	25 mg/kg daily	DMSO	i.p.	Radiotherapy (n = 5)	n = 8	n = 4	n = 6	—	—	(14)
Xanthinol Nicotinate	75 mg/kg	Saline	i.p.	Radio/chemo (n = 5/5)	n = 5	—	n = 5	—	—	(55)
Botulinum toxin	29 units/kg	Saline	i.t.	Radio/chemo (n = 6/6)	n = 8	—	n = 3	—	—	(56)
Carbogen	5 l/min	—	Inhalation	Radiotherapy (n = 6)	n = 10	—	—	n = 5	n = 5	(22)

endothelial growth factor (VEGF), SU5416 (13) and ZD6474 (14), thyroid hormones (15) and NO donors (16).

Dynamic contrast enhanced (DCE) MRI, intrinsic susceptibility weighted (BOLD) MRI and electronic paramagnetic resonance (EPR) oximetry all reflect tumor microenvironment hemodynamic variables that are known to influence tumor response; indeed:

- (1) DCE-MRI studies produce time-series images that enable pixel-by-pixel analysis of contrast kinetics within a tumor. Most methods of analyzing dynamic contrast-enhanced T_1 -weighted data acquired with low molecular contrast medium use a compartmental analysis to obtain some combination of the three principal parameters: the transfer constant K_{trans} in min^{-1} (volume transfer constant between blood plasma and EES), the rate constant K_{ep} in min^{-1} (rate constant between blood plasma and EES) and the volume of extravascular extracellular space (EES) per unit volume of tissue space, V_p (no unit) (17–20).
- (2) Magnetic resonance sequences that are based on the BOLD effect use the endogenous contrast agent deoxyhemoglobin as a source of contrast. Gradient echo images are usually employed for BOLD imaging. Both ΔR_2^* and relative change in signal intensity ($\% \Delta SI = SI_{post}/SI_{pre}$) are parameters that are proportional to the change in deoxyhemoglobin content (21–23).
- (3) Electron paramagnetic resonance (EPR) oximetry provides quantitative measurements of pO_2 over time under various physiological and pathophysiological conditions *in vivo* after implantation of a paramagnetic probe inside the tissue under study (6,24–26). This technique also provides the possibility of measuring oxygen consumption rate by cells *ex vivo* or *in vitro*.

The aim of the present work was to predict and monitor the efficacy of co-treatments to radio- and chemotherapy by noninvasive MR imaging. Ten different co-treatments were involved in this retrospective analysis of our previously published data, including NO-mediated co-treatments (insulin and isosorbide dinitrate), anti-inflammatory drugs (hydrocortisone, NS-398), anti-angiogenic agents (thalidomide, SU5416 and ZD6474), a vasoactive agent (xanthinol nicotinate), botulinum toxin and carbogen breathing (see Table 1). Eight MR markers (pO_2 , O_2 consumption, V_p , K_{trans} , K_{ep} , percentage of perfused vessels, BOLD SI and R_2^*) were tested for their ability to predict therapeutic outcome in experimental tumor models in order to help to qualify relevant imaging endpoints in the preclinical setting of cancer therapy.

2. RESULTS

All co-treatments induced an increase in tumor oxygenation. Figure 1 shows the windows of reoxygenation after each individual co-treatment in TLT (Fig. 1A) and FSall (Fig. 1B) tumors. This effect was explained by an increase in tumor blood flow for some of the co-treatments Isosorbide Dinitrate (IDN), thalidomide, Xanthinol Nicotinate (XN) and Botulinum toxin (BT), where the number of perfused voxels and/or K_{trans} , K_{ep} or V_p parameters was increased. Figure 2(A) shows typical maps of the percentage of perfused voxels in a tumor before and after treatment with BT. These data were computed for all co-treatments and are summarized in Fig. 2B, showing that only BT is able to increase the perfused area, whereas it is even decreased after administration

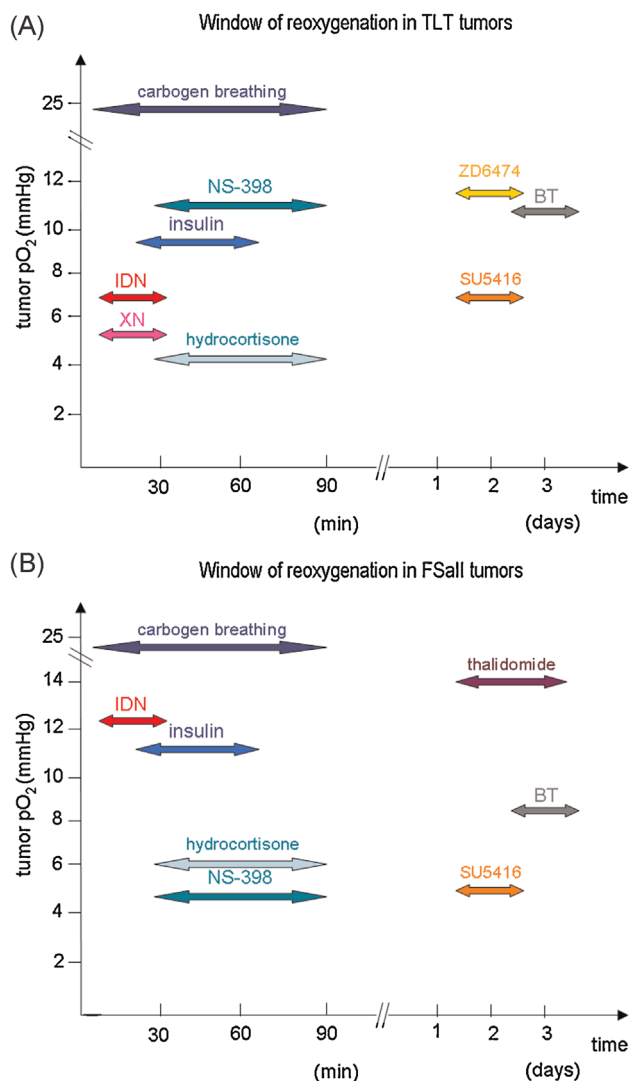


Figure 1. Schematic representation of the window of reoxygenation after administration of the co-treatments in TLT (A) and FSall (B) tumors.

of insulin, hydrocortisone, and NS-398. Figure 2C summarizes the evolution of the remaining DCE parameters: V_p is significantly increased after administration of XN or thalidomide, K_{trans} is modified by thalidomide only, and K_{ep} is enhanced by XN only. DCE-MRI therefore demonstrates a positive flow effect for the following co-treatments: BT, XN, and thalidomide.

However, other co-treatments (insulin, hydrocortisone, NS-398, SU5416 and ZD6474) resulted in a lack of change or even in a decrease in perfusion parameters. In this case, tumor cell oxygen consumption rate was estimated after each individual treatment. Figure 3 illustrates the ability of insulin, IDN, hydrocortisone, NS-398, SU5416 and ZD6474 to decrease tumor cell oxygen consumption rate by a factor of 2- to 3-fold, relative to untreated (control) cells. These data support the paradigm that playing on the oxygen consumption is as efficient as, or even more efficient than, targeting blood flow in order to improve oxygenation (8).

BOLD imaging was performed using vasoactive treatments, including IDN and carbogen breathing, showing increases in BOLD SI and R_2^* (Fig. 4A and B) (16,22). However, while BOLD imaging was performed for insulin and NS-398, two co-treatments that play on the consumption factor, there was no change in ΔR_2^* even though pO2 was modified (Fig. 4A and B). In addition, the percentage BOLD SI was even decreased due to a drop in S_0 . This means that, when consumption effects are involved, the BOLD markers might lead to a treatment being disregarded that still has potential. Figure 4C shows typical parametric maps after treatment with insulin.

Finally, the therapeutic relevance in terms of X-ray radiation therapy and chemotherapy with cyclophosphamide is shown in Fig. 5. The 'outcome' was considered in this study as the factor of increase in regrowth delay after radiation or chemotherapy, compared with the control group (without co-treatment in addition to the cytotoxic therapy). In Fig. 5, the positive responses are highlighted in green and the negative effects in red. An increase in flow (second column) is considered when one of the DCE parameter is significantly increased (V_p , K_{trans} , K_{ep} or percentage of perfused vessels). An increase in BOLD response means an increase in either BOLD signal intensity or T_2^* ($1/R_2^*$). A proper statistical analysis of each individual parameter has been performed in Table 2. We can observe that EPR oximetry is always predictive for radiotherapy, and most of the time for cyclophosphamide chemotherapy, except for one anti-angiogenic agent

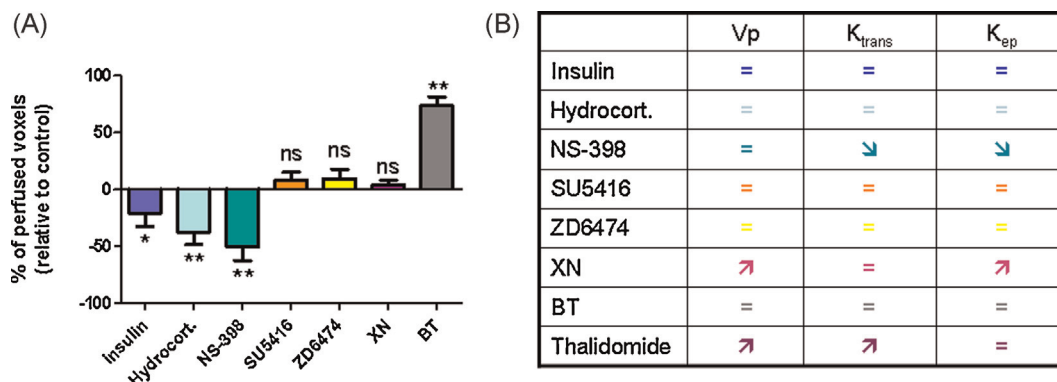


Figure 2. Effect of each co-treatment on tumor blood perfusion, assessed using DCE-MRI, showing changes in percentage of perfused vessels, V_p , K_{trans} and K_{ep} . (A) Typical example of an increase in percentage of perfused voxels after administration of Botulinum toxin; (B) bar graph representation of the effect of each co-treatment on the percentage of perfused voxels (* $p < 0.05$; ** $p < 0.01$, relative to untreated tumors). (C) Summary table of changes in the three DCE parameters (K_{trans} , V_p and K_{ep}), following administration of each co-treatment (= means statistically unchanged, arrows mean either increase or decreases in parameter that have been found significant, $p < 0.05$).

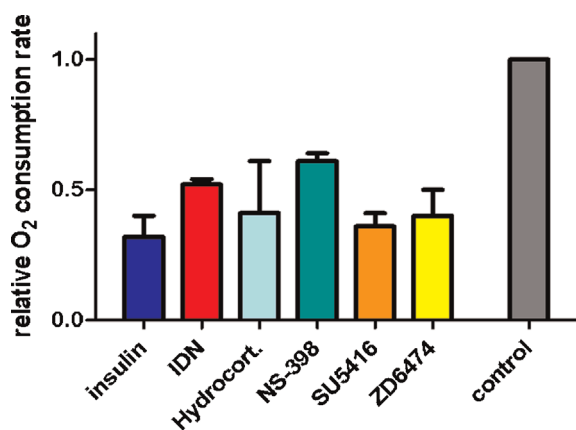


Figure 3. Change in oxygen consumption rate of tumor cells after administration of each co-treatment, relative to control (untreated) cells. All co-treatments presented in the figure significantly reduce the oxygen consumption rate of tumor cells ($p < 0.01$).

(SU5416). DCE-MRI is a poor marker regarding radiotherapy but is obviously and logically correlated with chemotherapy, since it conditions the access of the drug to the tumor. In particular, a lack of increase in blood flow is correlated with a lack of chemosensitization (in the case of SU5416), while all drugs able to increase tumor blood flow were correlated with an increase in chemosensitivity (thalidomide, XN and BT). The BOLD marker is not in accordance with radiation therapy outcome while a consumption effect is involved (insulin and NS-398), but correlates well if a flow effect is also involved (IDN). This method therefore does not provide additional predictive value to DCE-MRI.

The logistic regression of average values for each co-treatment (in terms of MR parameters and therapeutic outcome) allowed the predictive value of each marker to be assessed statistically. The statistic values are summarized in Table 2. Regarding radiotherapy outcome, the tumor pO_2 and the O_2 consumption are relevant predictive markers ($p < 0.05$). However, it is important to note that oxygen consumption was not evaluated for all co-treatments, and it is likely that this parameter would not be significant for treatments that only play on the blood flow. Regarding cyclophosphamide chemotherapy, V_p , K_{ep} and pO_2 are relevant predictive parameters ($p < 0.05$). Again, it is important to note that the therapeutic efficacy was not assessed for all treatments; the only treatments considered for chemotherapy were those able to open the vascular bed (anti-angiogenic agents in the normalization phase and botulinum toxin). pO_2 would probably not be predictive of chemotherapy outcome when flow parameters are decreased, as is the case for SU5416.

3. DISCUSSION

3.1. Imaging endpoints for radiation therapy

Our study qualified pO_2 as well as oxygen consumption as relevant imaging endpoints for radiation therapy outcome. The identification of *in vivo* pO_2 assessed by EPR oximetry as a relevant marker for radiation therapy outcome is in line with previously published data on the predictivity potential of EPR oximetry. Pogue *et al.* (27) evaluated the effect of photodynamic

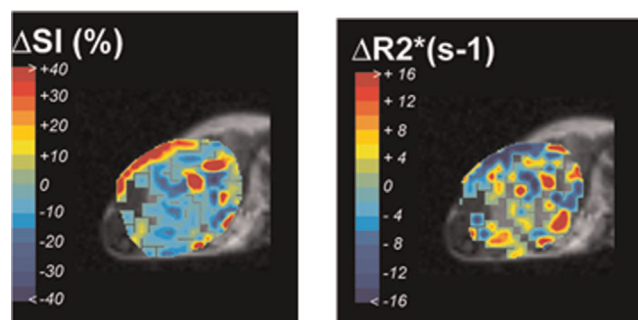
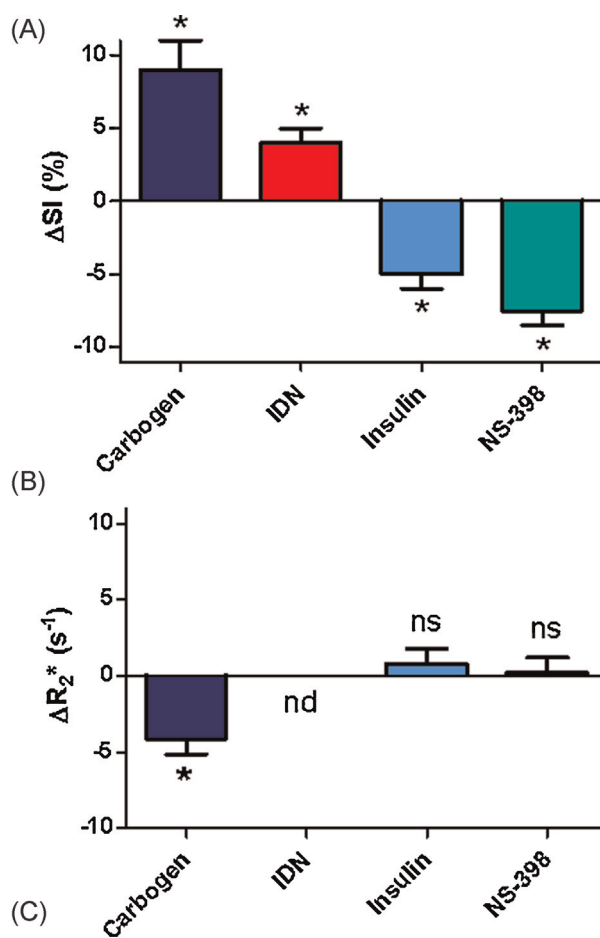


Figure 4. Change in BOLD signal intensity (SI) following administration of carbogen, IDN, insulin and NS-398. (A) Change in R_2^* following administration of carbogen, IDN, insulin and NS-398; (B) typical parametric maps of ΔSI and ΔR_2^* after administration of insulin; * $p < 0.05$, ** $p < 0.01$.

therapy (PDT) with verteporfin on radiation-induced fibrosarcoma. They observed an increase in pO_2 of up to 15.2 mmHg which correlated with the growth delay assay. Also, Hou *et al.* established a correlation between the effect of the allosteric hemoglobin modifier, efaroxiral, on tumor oxygenation and response to 4 Gy radiation therapy (28). Finally, Elas *et al.* (29) also found data arguing in favor of EPR oximetry as being a good predictor of tumor cure after radiation therapy in F5a tumors under both normal (air breathing) and clamped tumor conditions.

Oxygen consumption by tumor cells had not been considered as a marker of response until now. As stated earlier, this

	↑ pO ₂ ?	↑ « flow » ?	↓ O ₂ consumption ?	BOLD (fMRI) response?	Therapy outcome	
					Radio	Chemo
Insulin	YES	NO	YES	NO	+	nd
IDN	YES	YES	YES	YES	+	nd
Hydrocortisone	YES	NO	YES	nd	+	nd
NS-398	YES	NO	YES	NO	+	nd
Thalidomide	YES	YES	nd	nd	+	+
SU5416	YES	NO	YES	nd	+	-
ZD6474	YES	NO	YES	nd	+	nd
XN	YES	YES	nd	nd	+	+
BT	YES	YES	nd	nd	+	+
carbogen	YES	nd	nd	YES	+	nd

Figure 5. Summary tables of the therapeutic relevance of the co-treatments with regard to radiation therapy (A) or chemotherapy (B) with respect to the different MR endpoints. The outcome is considered as the factor of increase in regrowth delay after radiation or chemotherapy, compared with the control group. Positive responses are highlighted in green and negative effects in red. An increase in flow (second column) is considered when one of the DCE parameter is significantly increased (V_p , K_{trans} , K_{ep} or percentage of perfused vessels). An increase in BOLD response means an increase in either BOLD signal intensity or in T_2^* ($1/R_2^*$). Note that a proper statistical analysis on each individual parameter has been performed in Table 2.

parameter has to be interpreted with caution since all the co-treatments were not considered in terms of oxygen consumption (those that are able to open the vascular bed) and therefore data are lacking regarding this parameter. Also, we have to keep in mind that this marker is an *ex vivo* marker, in contrast to the other *in vivo* markers. Nevertheless, a new method has recently been developed to estimate oxygen consumption *in vivo* in experimental tumors (30).

Our study did not qualify BOLD (SI, R_2^*) or DCE (V_p , K_{trans} , K_{ep}) parameters as relevant imaging endpoints for radiation therapy. More specifically, the 'BOLD response' was not correlated with radiation therapy outcome when a consumption effect was identified, but correlated well for carbogen breathing. Usually, BOLD studies have reported good correlations in the past and our 'consumption' approach is the first to show a lack of correlation for BOLD imaging. Indeed, the BOLD signal was also assessed by different groups in the pre-clinical setting in order to establish correlations with the therapeutic outcome. The effect of RSR13, an allosteric modifier of hemoglobin was studied on NCI-H460

xenograft tumor response using BOLD-MRI and regrowth delays assay (31). RSR13 increased the SI ratio in a dose-dependent manner, with maximum increases occurring 30 min after RSR13 administration. This was correlated with an enhancement of radiation-induced growth delay of 2.8 while RSR13 was administered 30 min before a 10 Gy dose of radiation. Robinson's group further tested the prognostic potential of tumor R_2^* with respect to radiotherapeutic outcome on G3H prolactinomas and RIF-1 fibrosarcomas with animals breathing either air or carbogen during radiation (32). When the animals breathed carbogen during radiation, the growth delay was enhanced in the G3H prolactinomas, which also exhibited a large ΔR_2^* in response to carbogen. In contrast, the effect of 15 Gy on the RIF-1 fibrosarcomas, which gives a negligible ΔR_2^* in response to carbogen, showed a much smaller growth inhibition. These published data regarding carbogen breathing are therefore in line with our carbogen data.

Few studies have considered DCE-MRI as an imaging endpoint for radiation therapy outcome, since it is usually considered as an endpoint for the delivery of chemotherapeutic agents (see below). Nevertheless, Kiessling *et al.* (33) showed that DCE MRI parameter maps of Dunning rat prostate cancers were increased in terms of vascularization, K_{ep} and microvessel density, and this was correlated with the slowing of tumor growth after irradiation (33). More recently, the group of Dewhirst also showed that DCE-MRI parameters were predictive of thermoradiotherapy outcome in dogs with soft tissue sarcoma (34). On a clinical scale, Yamashita *et al.* showed that radiation therapy was more effective in tumors with higher tissue permeability than in those with lower tissue permeability (35). Similarly, George *et al.* (36) found that responsive tumors to chemoradiotherapy had higher pretreatment permeability values than non-responsive tumors. Prediction of radiotherapy outcome of carcinoma of the cervix was further evaluated on 50 patients (37): dynamic data correlated with patient outcome and patients with poorly enhancing tumors had significantly worse disease-specific survival.

Our data are therefore globally in line with the literature, although it is critical to keep in mind that a direct comparison is usually not possible because of inhomogeneity of data acquisition and analysis between different institutions. In particular, a

Table 2. Statistical analysis of the predictivity of each MR parameter (imaging endpoints) with respect to therapy outcome using logistic regression

MR parameter (marker)	Predictivity for radiotherapy outcome	Predictivity for chemotherapy outcome
pO ₂	$p < 0.01$ **	$p < 0.05$ *
O ₂ consumption	$p < 0.05$ *	nd
% perfused vessels	$p > 0.05$ n.s.	$p > 0.05$ n.s.
V_p	$p > 0.05$ n.s.	$p < 0.05$ *
K_{trans}	$p > 0.05$ n.s.	$p > 0.05$ n.s.
K_{ep}	$p > 0.05$ n.s.	$p < 0.05$ *
BOLD SI	$p > 0.05$ n.s.	n.d.
BOLD R_2^*	$p > 0.05$ n.s.	n.d.

n.s.: non significant; n.d.: not determined.

descriptive (semi-quantitative) analysis such as AUC (area under the curve) is difficult to compare with quantitative multiple compartment analysis of MR parameters that are more relevant to underlying physiological phenomenon.

3.2. Imaging endpoints for chemotherapy

Our study qualified V_p , K_{ep} and pO_2 as relevant imaging endpoints for chemotherapy outcome. The predictive value of DCE-MRI regarding the issue of chemotherapy has been considered in the past by many groups. It was used to monitor acute effects on tumor vascular permeability following inhibition of vascular endothelial growth factor-A (VEGF-A) signal transduction in PC-3 human prostate adenocarcinoma xenografts (38). Dose-related reductions in K_{trans} were evident following acute ZD6474 treatment and a correlation between this dose response and the growth inhibitory effect of ZD6474 following chronic treatment was also observed. This is quite different from what was observed in our studies using the same drug; however the timing and tumor models were also different. The antiangiogenic effect of SU6668 was assessed in HT29 human colon carcinoma in mice using DCE-MRI with large molecular contrast agent. SU6668 inhibited tumor growth, with 60% inhibition at 14 days of treatment, which was assessed early with DCE-MRI in terms of vascular permeability and fractional plasma volume at 24 h, and 3, 7, and 14 days time points (39). DCE-MRI with macromolecular contrast agent has further been used in HT-29 experimental tumors in order to assess the efficacy of the HIF-1 α inhibitor PX478 and to correlate with therapy outcome. A dramatic reduction in tumor blood vessel permeability was observed 2 h after treatment, and this was correlated with tumor regrowth (40).

On a clinical scale, the predictive value of DCE-MRI in terms of chemosensitivity in breast cancer patients was evaluated by Nagashima *et al.* (41). They demonstrated the significant correlation between pretreatment MRI data and tumor reduction by chemotherapy in breast cancer patients and suggested the possibility of defining good and non-responders prior to treatment. See *et al.* (42) also examined whether DCE-MRI done after two cycles of neoadjuvant 5-fluorouracil, epirubicin and cyclophosphamide chemotherapy could predict final clinical and pathologic response in primary breast cancers. They found that change in K_{trans} was the best predictor of pathologic non-response, whereas change in MRI-derived tumor size did not predict pathologic response. On the other hand, the Heerschap's group recently investigated the predictive value of DCE-MRI with Gd-DTPA for tumor response to first-line chemotherapy with 5-fluorouracil in patients with liver metastases of colorectal cancer (43). None of the kinetic parameters (K_{ep} , K_{trans} , V_e) was able to predict tumor response after 2 months, suggesting that the delivery of chemotherapy by tumor vasculature is not a major factor determining response in first-line treatment in liver metastasis.

Considering these studies, it is obvious that the predictive value of DCE markers is extremely dependent on the tumor model and the type of treatment, as well as the method of analysis. Also, a major point to take into consideration is the tumor heterogeneity, as the parameters are usually presented as mean or median values (of V_p , K_{trans} or K_{ep}). However, only the maps and histograms are able to integrate this heterogeneity aspect that is characteristic of all tumors. It would be difficult to find a single parameter that would reflect heterogeneity.

It is usually assumed that 'volume' parameters (V_p) are mainly determined by the volume fractions of the plasma and the interstitial distribution space, whereas K_{trans} and K_{ep} show a much higher dependency on perfusion and permeability than on interstitial volume and plasma volume (20). More specifically, K_{trans} is mainly governed by perfusion and K_{ep} is determined to a larger extent by permeability. Nevertheless, physiological interpretation of the estimated model parameters should be done with care, as methods of data acquisition and kinetic modeling can result in completely different values and uncertainties on each parameter, particularly with regard to the estimation of the AIF (arterial input function) (20).

Our analysis also points out that the pO_2 could be a predictive marker for chemotherapy outcome, which is quite intuitive for treatments that are able to improve blood flow (and therefore pO_2). However, other mechanisms can also be responsible for improved oxygenation (such as consumption effects), and our table is lacking some data to qualify this marker as a surrogate imaging endpoint for chemotherapy.

The assessment of absolute values of tumor pO_2 *in vivo* is of critical importance for radiation therapy planning and monitoring. The recent developments in EPR imaging (oxygen mapping) will allow the tumor heterogeneity to be taken into account, which will add a significant value for this technique to be considered as a surrogate imaging endpoint. Indeed, this will allow identification of potential resistant zones. The pO_2 biomarker can be evaluated quantitatively *in vivo* (in experimental models) using EPR oximetry (spectroscopy and imaging), but also with ^{19}F -MRI, and DNP (dynamic nuclear polarization) oximetry (6,24–26,44,45). Finally, hypoxia radiotracers are not convenient to monitor acute changes in tumor oxygenation since the measurement would require at least 2 days of experiment because of the kinetics of nitroimidazoles (one measurement in order to assess the basal pO_2 and one measurement after washout to assess the efficacy of the co-treatment).

The assessment of relative changes in blood flow is determinant for tumor response to chemotherapy. Those changes can be assessed *in vivo* using DCE-MRI (17–20), or 'non-MR' methods, including CT with iodinated contrast agent, and nuclear medicine (PET/SPECT) (46). It is important to note that the basal blood flow value has no prognostic value in this context; only 'delta' values extracted from dynamic studies are relevant, in contrast to the absolute basal pO_2 value, which can give predictive data. Nevertheless, chemotherapeutic drugs containing a fluorine can be monitored dynamically using ^{19}F -MRS to see their accumulation into the tumor (47,48).

4. CONCLUSION

By computing data acquired on 10 different co-treatments in experimental tumors (656 animals), we were able to determine which MR markers are robust in terms of predictive value of therapy outcome. From our statistical analysis, we can conclude that: (i) pO_2 is a qualified imaging endpoint for radiotherapy, and (ii) V_p and K_{ep} are qualified imaging endpoints for chemotherapy, despite the predictive value of DCE markers being extremely dependent on tumor model, type of treatment, and kinetic modeling. Moreover, oxygen consumption and pO_2 were also found to be significant regarding radiation therapy and chemotherapy, respectively, but this should be interpreted with caution since some data are missing that would enable us to draw strong

conclusions. Also, it is important to keep in mind that oxygen consumption is an *ex vivo* marker, in contrast to the other *in vivo* markers. Of interest, both DCE and BOLD parameters failed to be predictive regarding radiation therapy outcome, particularly when a consumption effect was involved. Therefore, BOLD and DCE markers could lead to wrong interpretation of the potential use of a compound as a co-treatment for radiotherapy.

Our retrospective analysis shows the limitations of different MR techniques (endpoints) in terms of surrogate markers of tumor response to therapy. It is obvious that the analysis should be enriched by a further comparison with other (emerging) MR markers, such as ADC_w in diffusion imaging (DW-MRI), choline spectroscopy, or by comparison with other imaging modalities, such as FDG-PET or FLT-PET. This study can help to define relevant imaging endpoints in the preclinical setting of cancer therapy and suggests the need to translate those markers to the clinic for theranostic purposes.

5. MATERIALS AND METHODS

5.1. Animal tumor models

Two different tumor models were implanted in the thigh of mice: a transplantable liver tumor model (TLT) (49) on NMRI mice and the syngeneic FSaII tumor model (50) on C3H mice. For inoculation, approximately 10^6 cells in 0.1 ml of media were injected intramuscularly into the right leg of 5 week-old male mice. Mice developed palpable tumors within a week of inoculation. Tumors were allowed to grow up to 8 mm in diameter prior to experimentation. Animals were anesthetized either by an i.p. injection of ketamine (80 mg/kg)/xylazine (8 mg/kg) and maintained with ketamine alone (30 mg/kg); or by inhalation of isoflurane mixed with 21% oxygen in a continuous flow (1.5 l/h), delivered by a nose cone. In this case, induction of anesthesia was done using 3% isoflurane. It was then stabilized at 1.8% for a minimum of 15 minutes before any measurement. The temperature of the animals was kept constant using IR light or by flushing warm air in the MR magnet. EPR oximetry experiments were systematically performed on TLT and FSa II tumors.

5.2. Co-treatments

All the co-treatments and respective doses as well as injection routes are summarized in Table 1. Insulin (Actrapid HM) was from Novo Nordisk, Bagsvaerd, Denmark; isosorbide dinitrate (Cedocard, 1 mg/ml) was from Byk Belga, Brussels, Belgium; hydrocortisone (Solu-Cortef) was from Pharmacia, Pfizer, Brussels, Belgium; NS-398 [N-[2(cyclohexyloxy) 4-nitrophenyl-methanesulfonamide]] was from Alexis Biochemicals, Zandhoven, Belgium; racemic thalidomide was from (Sigma-Aldrich, Bornem, Belgium); SU5416 was from Sigma-Aldrich; Vandetanib (ZD6474) was from Astra Zeneca (Macclesfield, UK); and BoNT-A (Botox) was from Allergan, (Antwerp, Belgium).

5.3. Cytotoxic treatments of tumors

All co-treatments were tested in combination with radiotherapy or chemotherapy for estimation of the therapeutic relevance and correlation with the MR markers of response. Irradiation was performed in the time window during which intratumoral pO₂ was maximal for each co-treatment. The right leg was locally irradiated with 10 Gy of 250 kV X-rays (RT 250; Philips Medical

Systems). The tumor was centered in a 3 cm diameter circular irradiation field. A single dose irradiation was performed. At a second time, chemotherapy was performed for treatments that were able to open the vascular bed (antiangiogenic agents in normalization phase, and BT). For that purpose, the alkylating agent cyclophosphamide was dissolved in saline and injected intraperitoneally at the suboptimal dose of 50 mg/kg at the time of maximum of increase in blood flow. The relevance studies included several groups: (i) control groups (no cytotoxic treatments, administration of the co-treatments and their respective vehicles); and (ii) 'X-ray' or cyclophosphamide groups, alone or in combination with a co-treatment. After treatment, the tumor growth was determined daily by measuring tumor diameter until they reached a size of 16 mm, at which time the mice were sacrificed. A linear fit was performed between initial tumor size (7.5 ± 1 mm) and 16 mm, which allowed determination of the time to reach a particular size for each mouse. The regrowth delay was then considered as the time to reach 12 mm in tumor diameter. The factor of increase was regrowth delay for the treated group (co-treatment + irradiation or cyclophosphamide) vs the control group (irradiated or treated with cyclophosphamide but without co-treatment).

5.4. Experimental design

Tumor pO₂ was systematically assessed on both tumor models, TLT and FSaII, except for thalidomide (FSaII model only) and XN (TLT model only). The remaining MR endpoints (DCE-MRI, *ex vivo* EPR and BOLD MRI) and therapeutic relevance experiments were performed on the FSaII tumor model for insulin, IDN, hydrocortisone, NS-398, SU5416, thalidomide, BT and carbogen; and on the TLT tumor model for ZD6474 and XN.

5.5. Tumor oxygenation

Electronic paramagnetic resonance oximetry, using charcoal (CX0670-1, EM Science, Gibbstown, NJ, USA) as the oxygen sensitive probe, was used to evaluate the tumor oxygenation (6). EPR oximetry relies on the oxygen-dependent broadening of the EPR linewidth of a paramagnetic oxygen sensor implanted in the tumor. This technique is designed for continuous measurement of the local pO₂ without altering the local oxygen concentration, and allows repeated measurements from the same site over long periods of time. EPR spectra were recorded using an EPR spectrometer (Magnetech, Berlin, Germany) with a low-frequency microwave bridge operating at 1.2 GHz and extended loop resonator. Mice were injected once in the center of the tumor using a 26g needle 1 day before measurement using the suspension of charcoal (suspension in saline containing 3% arabic gum, 100 mg/ml, 50 μ l injected, 1–25 μ m particle size). The tumor under study was placed in the center of the extended loop resonator, of which the sensitive volume extended 1 cm into the tumor mass, using a protocol described previously. The localized EPR measurements correspond to an average of pO₂ values in a volume of ~ 10 mm³ (6).

5.6. Tumor cell oxygen consumption rate

The method developed by James *et al.* was used (51). All of the spectra were recorded on a Bruker EMX EPR spectrometer operating at 9 GHz. Mice were first treated with one of the co-treatment *in vivo*. At the time of maximum reoxygenation, tumors were excised, trypsinized for 30 min, and cell viability

determined. Cells (2×10^7 /ml) were suspended in 10% dextran in complete medium. A neutral nitroxide, 15N 4-oxo-2,2,6,6-tetramethylpiperidine-d16-15N-1-oxyl at 0.2 mM (CDN Isotopes, Pointe-Claire, Quebec, Canada), was added to 100 μ l aliquots of tumor cells that were then drawn into glass capillary tubes. The probe (0.2 mM in 20% dextran in complete medium) was calibrated at various O_2 between 100% nitrogen and air so that the linewidth measurements could be related to O_2 at any value. Nitrogen and air were mixed in an Aalborg gas mixer, and the oxygen content was analyzed using a servomex oxygen analyzer OA540. The sealed tubes were placed into quartz ESR tubes, and samples were maintained at 37°C. As shown by the resulting linewidth reports on O_2 , oxygen consumption rates were obtained by measuring the O_2 in the closed tube over time and finding the slope of the resulting linear plot.

5.7. Tumor blood flow parameters

The perfusion was monitored in the time window during which intratumoral pO_2 was maximal after administration of the co-treatment, as determined by EPR oximetry. The perfusion parameters were monitored via single-slice dynamic contrast-enhanced MRI at 4.7 T (200 MHz, 1H), on a 40 cm inner diameter horizontal bore system (Bruker Biospec, Ettlingen, Germany), using the rapid-clearance blood pool agent P792 (Vistarem[®], Guerbet, Roissy, France) (52). High-resolution multi-slice T_2 -weighted spin echo anatomic imaging was performed just before dynamic contrast-enhanced imaging. For that purpose, proton density-weighted (PDw) images were acquired with the following parameters: $TR = 8$ s, $TE = 4.9$ ms, number of averages (NA) = 2, flip angle = 90°, FOV = 4 cm, slice thickness = 1.6 mm, matrix = 64×64 , two slices (one slice through the kidneys and one through the center of the tumor).

For DCE T_1 -weighted imaging, a gradient-recalled echo sequence was used with the following parameters: $TR = 40$ ms, $TE = 4.9$ ms, NA = 1, flip angle = 90°, geometry parameters = same as for the PDw sequence, scan time per image = 2.56 s. The contrast agent P792 (Vistarem[®]; Laboratoire Guerbet, Aulnay sous Bois, France) was injected intravenously as a bolus (injection duration = 2 s) at a dose of 0.042 mmol Gd/kg (50 μ l/40 g mouse). The DCE imaging protocol was as follows: 12 baseline images were acquired, and then P792 was injected and the enhancement kinetics were continuously monitored for 8 min (200 total scans) in order to track the fast washing kinetics. Immediately after this, a slower DCE data set was acquired to monitor the washout of the contrast agent. For this second set, 60 scans were acquired at a temporal resolution of 60 s (NA = 24, 1 h total).

For postprocessing, tumor voxels that showed no signal enhancement, a linear increase of SI, or atypical signal enhancement curves were excluded by means of a power spectrum analysis and cluster analysis. The tracer concentration changes were fitted to a two-compartment pharmacokinetic model using an arterial input function derived from kidney data as described previously. Pixel-by-pixel values for K_{trans} (influx volume transfer constant, from plasma into the interstitial space, units of min^{-1}), V_p (blood plasma volume per unit volume of tissue, unitless) and K_{ep} (fractional rate of efflux from the interstitial space back to blood, units of min^{-1}) in the tumor were derived from this model. Statistical significance for V_p or K_{trans} identified the percentage of 'perfused' tumor pixels (i.e. pixels to which the contrast agent P792 had access) (53).

5.8. Tumor BOLD parameters

A multi-echo GRE sequence was used for the calculation of the GRE signal intensity (T_2^* GRE MRI), R_2^* and S_0 and on a pixel-by-pixel basis in each tumor. The sequence parameters were $TR = 200$ ms, six echoes with an echo spacing of 5 ms ($TE = 5, 10, 15, 20, 25, 30$ ms), spectral width = 25 kHz, flip angle = 45°, matrix size = 64×64 , FOV = 4 cm, slice thickness = 1.6 mm, NA = 10, total acquisition time = 128 s. MRI data were acquired continuously for 1 h 45 min with the administration of the co-treatment at repetition 5. For each repetition, a monoexponential function was used to fit the GRE signal as a function of echo time. The GRE signal intensity (SI) was taken to be the GRE signal at $TE = 20$ ms. The parameters R_2^* ($= 1/T_2^*$) and S_0 (theoretical GRE signal at $TE = 0$ ms) were determined as fit parameters in the monoexponential function (54). The relative changes in GRE signal intensity (% Δ SI) and in S_0 were calculated. The change in R_2^* (ΔR_2^*) and % Δ SI are parameters that are proportional to the change in deoxyhemoglobin content. These two parameters are independent of native tissue R_2^* , unlike ΔT_2^* and the absolute change in SI. Therefore, treated and control groups were compared in terms of % Δ SI, ΔR_2^* and the relative change in S_0 .

5.9. Statistical analysis

Mean values of MR parameters were compared using one way ANOVA for all co-treatments relative to control, $p < 0.05$ * and $p < 0.01$ **. The predictivity of each MR parameter with respect to the issue of radio and/or chemotherapy was analyzed by logistic regression with JMP using published averaged values for each co-treatment. Multivariate analysis was not possible due to the lack of data for some parameters (Table 2).

Acknowledgements

This work was supported by grants from the Belgian National Fund for Scientific Research, the Televie, the Fonds Joseph Maisin, the Saint-Luc Foundation, The 'Fondation contre le cancer', the 'Actions de Recherches Concertées-Communauté Française de Belgique-ARC 09/14-020' and the 'Pôle d'attraction Interuniversitaire PAI VI (P6/38)'. B.J. is a research associate of the FNRS.

References

- Gillies RJ, Raghunand N, Karczmar GS, Bhujwala ZM. MRI of the tumor microenvironment. *J Magn. Reson. Imag* 2002; 16: 430–450.
- Tatum JL, Kelloff GJ, Gillies RJ, Arbeit JM, Brown JM, Chao KS, Chapman JD, Eckelman WC, Fyles AW, Giaccia AJ, Hill RP, Koch CJ, Krishna MC, Krohn KA, Lewis JS, Mason RP, Melillo G, Padhani AR, Powis G, Rajendran JG, Reba R, Robinson SP, Semenza GL, Swartz HM, Vaupel P, Yang D, Croft B, Hoffman J, Liu G, Stone H, Sullivan D. Hypoxia: importance in tumor biology, noninvasive measurement by imaging, and value of its measurement in the management of cancer therapy. *Int J Radiat Biol* 2006; 82: 699–757.
- Höckel M, Vaupel P. Tumor hypoxia: definitions and current clinical, biologic, and molecular aspects. *J Natl Cancer Inst* 2001; 93: 266–276.
- Overgaard J. Hypoxic radiosensitization: adored and ignored. *J Clin Oncol* 2007; 25: 4066–4074.
- Evelhoch JL, Gillies RJ, Karczmar GS, Koutcher JA, Maxwell RJ, Nalcioglu O, Raghunand N, Ronen SM, Ross BD, Swartz HM. Applications of magnetic resonance in model systems: cancer therapeutics. *Neoplasia* 2000; 2: 152–165.

6. Gallez B, Baudelet C, Jordan BF. Assessment of tumor oxygenation by electron paramagnetic resonance: principles and applications. *NMR Biomed* 2004; 17: 240–262.
7. Sonveaux P. Provascular strategy: targeting functional adaptations of mature blood vessels in tumors to selectively influence the tumor vascular reactivity and improve cancer treatment. *Radiother Oncol* 2008; 86: 300–313.
8. Secomb TW, Hsu R, Ong ET, Gross JF, Dewhirst MW. Analysis of the effects of oxygen supply and demand on hypoxic fraction in tumors. *Acta Oncol* 1995; 34: 313–316.
9. Biaglow JE, Manevich Y, Leeper D, Chance B, Dewhirst MW, Jenkins WT, Tuttle SW, Wroblewski K, Glickson JD, Stevens C, Evans SM. MIBG inhibits respiration: potential for radio- and hyperthermic sensitization. *Int J Radiat Oncol Biol Phys* 1998; 42: 871–876.
10. Jordan BF, Grégoire V, Demeure RJ, Sonveaux P, Feron O, O'Hara J, Vanhulle VP, Delzenne N, Gallez B. Insulin increases the sensitivity of tumors to irradiation: involvement of an increase in tumor oxygenation mediated by a nitric oxide-dependent decrease of the tumor cells oxygen consumption. *Cancer Res* 2002; 62: 3555–3561.
11. Crockart N, Radermacher K, Jordan BF, Baudelet C, Cron GO, Grégoire V, Beghein N, Bouzin C, Feron O, Gallez B. Tumor radiosensitization by antiinflammatory drugs: evidence for a new mechanism involving the oxygen effect. *Cancer Res* 2005; 65: 7911–7916.
12. Crockart N, Jordan BF, Baudelet C, Cron GO, Hotton J, Radermacher K, Grégoire V, Beghein N, Martinive P, Bouzin C, Feron O, Gallez B. Glucocorticoids modulate tumor radiation response through a decrease in tumor oxygen consumption. *Clin Cancer Res* 2007; 13: 630–635.
13. Ansiaux R, Baudelet C, Jordan BF, Crockart N, Martinive P, DeWever J, Grégoire V, Feron O, Gallez B. Mechanism of reoxygenation after antiangiogenic therapy using SU5416 and its importance for guiding combined antitumor therapy. *Cancer Res* 2006; 66: 9698–9704.
14. Ansiaux R, Dewever J, Gregoire V, Feron O, Jordan BF, Gallez B. Decrease in tumor cell oxygen consumption after treatment by vandetanib (ZD6474) and its effects on response to radiotherapy. *Radiat. Res* 2009; 172: 584–591.
15. Jordan BF, Christian N, Crockart N, Grégoire V, Feron O, Gallez B. Thyroid status is a key modulator of tumor oxygenation: implication for radiation therapy. *Radiat Res* 2007; 168: 428–432.
16. Jordan BF, Misson P, Demeure R, Baudelet C, Beghein N, Gallez B. Changes in tumor oxygenation/perfusion induced by the no donor, isosorbide dinitrate, in comparison with carbogen: monitoring by EPR and MRI. *Int J Radiat Oncol Biol Phys* 2000; 48: 565–570.
17. Tofts PS, Brix G, Buckley DL, Evelhoch JL, Henderson E, Knopp MV, Larsson HB, Lee TY, Mayr NA, Parker GJ, Port RE, Taylor J, Weisskoff RM. Estimating kinetic parameters from dynamic contrast-enhanced T(1)-weighted MRI of a diffusible tracer: standardized quantities and symbols. *J Magn Reson Imag* 1999; 10: 223–232.
18. Padhani AR, Leach MO. Antivascular cancer treatments: functional assessments by dynamic contrast-enhanced magnetic resonance imaging. *Abdom Imag* 2005; 30: 324–341.
19. Jordan BF, Gallon JP, Gillies RJ. Post-treatment changes in tumor microenvironment: dynamic contrast enhanced and diffusion weighted magnetic resonance imaging. *Cancer Imag*. 2008; 2: 235–248.
20. Zwick S, Strecker R, Kiselev V, Gall P, Huppert J, Palmowski M, Lederle W, Woenne EC, Hengerer A, Taupitz M, Semmler W, Kiessling F. Assessment of vascular remodeling under antiangiogenic therapy using DCE-MRI and vessel size imaging. *J Magn Reson Imag* 2009; 29: 1125–1133.
21. Howe FA, Robinson SP, McIntyre DJ, Stubbs M, Griffiths JR. Issues in flow and oxygenation dependent contrast (FLOOD) imaging of tumours. *NMR Biomed* 2001; 14: 497–506.
22. Baudelet C, Gallez B. How does blood oxygen level-dependent (BOLD) contrast correlate with oxygen partial pressure (pO₂) inside tumors? *Magn Reson Med* 2002; 48(6): 980–986.
23. Robinson SP, Rijken PF, Howe FA, McSheehy PM, van der Sanden BP, Heerschap A, Stubbs M, van der Kogel AJ, Griffiths JR. Tumor vascular architecture and function evaluated by non-invasive susceptibility MRI methods and immunohistochemistry. *J Magn Reson Imag* 2003; 17: 445–454.
24. Swartz HM, Clarkson RB. The measurement of oxygen in vivo using EPR techniques. *Phys Med Biol* 1998; 43: 1957–1975.
25. Krishna MC, Devasahayam N, Cook JA, Subramanian S, Kuppusamy P, Mitchell JB. Electron paramagnetic resonance for small animal imaging applications. *ILAR J* 2001; 42: 209–218.
26. Vikram DS, Zweier JL, Kuppusamy P. Methods for noninvasive imaging of tissue hypoxia. *Antioxid Redox Signal* 2007; 9: 1745–1756.
27. Pogue BW, O'Hara JA, Demidenko E, Wilmot CM, Goodwin IA, Chen B, Swartz HM, Hasan T. Photodynamic therapy with verteporfin in the radiation-induced fibrosarcoma-1 tumor causes enhanced radiation sensitivity. *Cancer Res* 2003; 63: 1025–1033.
28. Hou H, Khan N, Grinberg OY, Yu H, Grinberg SA, Lu S, Demidenko E, Steffen RP, Swartz HM. The effects of Efaroxyn (efaproxiral) on subcutaneous RIF-1 tumor oxygenation and enhancement of radiotherapy-mediated inhibition of tumor growth in mice. *Radiat Res* 2007; 168: 218–225.
29. Elas M, Bell R, Hleihel D, Barth ED, McFaul C, Haney CR, Bielanska J, Pustelny K, Ahn KH, Pelizzari CA, Kocherginsky M, Halpern HJ. Electron paramagnetic resonance oxygen image hypoxic fraction plus radiation dose strongly correlates with tumor cure in F5a fibrosarcomas. *Int J Radiat Oncol Biol Phys* 2008; 71: 542–549.
30. Diepart C, Jordan BF, Gallez B. A New EPR oximetry protocol to estimate the tissue oxygen consumption in vivo. *Radiat Res* 2009; 172: 220–225.
31. Amorino GP, Lee H, Holburn GE, Paschal CB, Hercules SK, Shyr Y, Steffen RP, Choy H. Enhancement of tumor oxygenation and radiation response by the allosteric effector of hemoglobin, RSR13. *Radiat Res* 2001; 156: 294–300.
32. Rodrigues LM, Howe FA, Griffiths JR, Robinson SP. Tumor R₂* is a prognostic indicator of acute radiotherapeutic response in rodent tumors. *J Magn Reson Imag* 2004; 19: 482–488.
33. Kiessling F, Huber PE, Grobholz R, Heilmann M, Meding J, Lichy MP, Fink C, Krix M, Peschke P, Schlemmer HP. Dynamic magnetic resonance tomography and proton magnetic resonance spectroscopy of prostate cancers in rats treated by radiotherapy. *Invest Radiol* 2004; 39: 34–44.
34. Viglianti BL, Lora-Michiels M, Poulson JM, Lan L, Yu D, Sanders L, Craciunescu O, Vujaskovic Z, Thrall DE, Macfall J, Charles CH, Wong T, Dewhirst MW. Dynamic contrast-enhanced magnetic resonance imaging as a predictor of clinical outcome in canine spontaneous soft tissue sarcomas treated with thermoradiotherapy. *Clin. Cancer Res* 2009; 15: 4993–5001.
35. Yamashita Y, Baba T, Baba Y, Nishimura R, Ikeda S, Takahashi M, Ohtake H, Okamura H. Dynamic contrast-enhanced MR imaging of uterine cervical cancer: pharmacokinetic analysis with histopathologic correlation and its importance in predicting the outcome of radiation therapy. *Radiology* 2000; 216: 803–809.
36. George ML, Dzik-Jurasz AS, Padhani AR, Brown G, Tait DM, Eccles SA, Swift RI. Non-invasive methods of assessing angiogenesis and their value in predicting response to treatment in colorectal cancer. *Br J Surg* 2001; 88: 1628–1636.
37. Lancaster JA, Carrington BM, Sykes JR, Jones AP, Todd SM, Cooper R, Buckley DL, Davidson SE, Logue JP, Hunter RD, West CM. Prediction of radiotherapy outcome using dynamic contrast enhanced MRI of carcinoma of the cervix. *Int. J. Radiat. Oncol. Biol. Phys* 2002; 54: 759–767.
38. Checkley D, Tessier JJ, Kendrew J, Waterton JC, Wedge SR. Use of dynamic contrast-enhanced MRI to evaluate acute treatment with ZD6474, a VEGF signalling inhibitor, in PC-3 prostate tumours. *Br J Cancer* 2003; 89: 1889–1895.
39. Marzola P, Degrassi A, Calderan L, Farace P, Crescimanno C, Nicolato E, Giusti A, Pesenti E, Terron A, Sbarbati A, Abrams T, Murray L, Osculati F. In vivo assessment of antiangiogenic activity of SU6668 in an experimental colon carcinoma model. *Clin Cancer Res* 2004; 10: 739–750.
40. Jordan BF, Runquist M, Raghunand N, Baker A, Williams R, Kirkpatrick L, Powis G, Gillies RJ. Dynamic contrast-enhanced and diffusion MRI show rapid and dramatic changes in tumor microenvironment in response to inhibition of HIF-1alpha using PX-478. *Neoplasia* 2005; 7: 475–485.
41. Nagashima T, Sakakibara M, Nakamura R, Arai M, Kadowaki M, Kazama T, Nakatani Y, Koda K, Miyazaki M. Dynamic enhanced

- MRI predicts chemosensitivity in breast cancer patients. *Eur J Radiol* 2006; 60: 270–274.
42. Ah-See ML, Makris A, Taylor NJ, Harrison M, Richman PI, Burcombe RJ, Stirling JJ, d'Arcy JA, Collins DJ, Pittam MR, Ravichandran D, Padhani AR. Early changes in functional dynamic magnetic resonance imaging predict for pathologic response to neoadjuvant chemotherapy in primary breast cancer. *Clin Cancer Res* 2008; 14: 6580–6589.
 43. van Laarhoven HW, Klomp DW, Rijpkema M, Kamm YL, Wagener DJ, Barentsz JO, Punt CJ, Heerschap A. Prediction of chemotherapeutic response of colorectal liver metastases with dynamic gadolinium-DTPA-enhanced MRI and localized ¹⁹F MRS pharmacokinetic studies of 5-fluorouracil. *NMR Biomed* 2007; 20: 128–140.
 44. Mason RP, Hunjan S, Constantinescu A, Song Y, Zhao D, Hahn EW, Antich PP, Peschke P. Tumor oximetry: comparison of ¹⁹F MR EPI and electrodes. *Adv Exp Med Biol* 2003; 530: 19–27.
 45. Clarkson RB, Odintsov BM, Ceroke PJ, Ardenkjaer-Larsen JH, Fruianu M, Belford RL. Electron paramagnetic resonance and dynamic nuclear polarization of char suspensions: surface science and oximetry. *Phys Med Biol* 1998; 43: 1907–1920.
 46. Jennings D, Raghunand N, Gillies RJ. Imaging hemodynamics. *Cancer Metastasis Rev* 2008; 27: 589–613.
 47. Cron GO, Beghein N, Ansiaux R, Martinive P, Feron O, Gallez B. ¹⁹F NMR in vivo spectroscopy reflects the effectiveness of perfusion-enhancing vascular modifiers for improving gemcitabine chemotherapy. *Magn Reson Med* 2008; 59: 19–27.
 48. Schlemmer HP, Becker M, Bachert P, Dietz A, Rudat V, Vanselow B, Wollensack P, Zuna I, Knopp MV, Weidauer H, Wannemacher M, van Kaick G. Alterations of intratumoral pharmacokinetics of 5-fluorouracil in head and neck carcinoma during simultaneous radiochemotherapy. *Cancer Res* 1999; 59: 2363–2369.
 49. Taper HS, Woolley GW, Teller MN, Lardis MP. A new transplantable mouse liver tumor of spontaneous origin. *Cancer Res* 1966; 26: 143–148.
 50. Volpe JP, Hunter N, Basic I, Milas L. Metastatic properties of murine sarcomas and carcinomas I. positive correlation with lung colonization and lack of correlation with s.c. tumor take. *Clin. Expl. Metastasis* 1985; 3: 281–294.
 51. James PE, Jackson SK, Grinberg OY, Swartz HM. The effects of endotoxin on oxygen consumption of various cell types in vitro: an EPR oximetry study. *Free Radic Biol Med* 1995; 18: 641–647.
 52. Fan X, Medved M, River JN, Zamora M, Corot C, Robert P, Bourrinet P, Lipton M, Culp RM, Karczmar GS. New model for analysis of dynamic contrast-enhanced MRI data distinguishes metastatic from nonmetastatic transplanted rodent prostate tumors. *Magn Reson Med* 2004; 51: 487–494.
 53. Baudelet C, Ansiaux R, Jordan BF, Havaux X, Macq B, Gallez B. Physiological noise in murine solid tumors using T₂*-weighted gradient-echo imaging: a marker of tumour acute hypoxia? *Phys Med Biol* 2004; 49: 3389–3411.
 54. Ansiaux R, Baudelet C, Jordan BF, Beghein N, Sonveaux P, De Wever J, Martinive P, Grégoire V, Feron O, Gallez B. Thalidomide radiosensitizes tumors through early changes in the tumor microenvironment. *Clin Cancer Res* 2005; 11: 743–750.
 55. Segers J, Crockart N, Danhier P, Grégoire V, Jordan BF, Gallez B. Use of xanthinol nicotinate as a co-treatment for radio- and chemotherapy in experimental tumors. *Int J Cancer* 2010; 126(2): 583–588.
 56. Ansiaux R, Baudelet C, Cron GO, Segers J, Dessy C, Martinive P, De Wever J, Verrax J, Wauthier V, Beghein N, Grégoire V, Buc Calderon P, Feron O, Gallez B. Botulinum toxin potentiates cancer radiotherapy and chemotherapy. *Clin Cancer Res* 2006; 12: 1276–1283.